Biomaterials Advances xxx (xxxx) 213395

Contents lists available at ScienceDirect

Biomaterials Advances

journal homepage: www.elsevier.com

Journal Cover Image

Graphene quantum dots-hybrid hydrogel as an avant-garde biomimetic scaffold for diabetic wound healing

Kumar Shivam [a, 1], Abhyavartin Selvam [a, b, 1], Sujata Sangam [c, 1], Misba Majood [a, 1], Siddhartha Pahari [a], Ranjan Patra [a], Arun K. Sharma [d, **], Monalisa Mukherjee [a, c, *]

[a] Amity Institute of Click Chemistry Research and Studies, Amity University, Noida, Uttar Pradesh 201313, India
[b] Amity Institute of Nanotechnology, Amity University, Noida, Uttar Pradesh 201313, India
[c] Amity Institute of Biotechnology, Amity University, Noida, Uttar Pradesh 201313, India
[d] Amity Institute of Pharmacy, Amity University, Gurugram, Haryana 122413, India

ARTICLE INFO

Keywords:
Diabetic wound healing
Hybrid hydrogel
Graphene quantum dots
Biomimetic scaffold

ABSTRACT

In the age of fathoming biomedical predicaments, ardently emerged the field of materiobiology to effectively counter the archetypal and outdated therapies. Correspondingly, the subpar activity of the over-the-counter wound dressing pharmaceuticals have been dominated with the implementation of biocompatible, water-retaining exotic hydrogels to facilitate accelerated diabetic wound healing. Considering a strategy to develop a pragmatic biomimetic scaffold having the ability of dynamic wound healing with diminutive inflammation, we investigated the creation of graphene quantum dot (GQD)-polyacrylic acid (PAA) hybrid hydrogel. We observe appropriate percentage of GQD incorporation in PAA to demonstrate lower pro-inflammatory cytokines, interleukin (IL-6), and tumour necrosis factor (TNF-α) along with higher anti-inflammatory (IL-10) expressions in contrast to natural and standard controls. Likewise, histological examinations corresponding to the in-vitro and in-vivo toxicological analysis of GQD-PAA manifested to be a non-toxic, biocompatible saviour of diabetic wounds. This hybrid hydrogel reports the quickest diabetic wound healing of 13 days. Additionally, the hybrid hydrogel also demonstrates salient antibacterial activity against *E. coli*. We explore a multifaceted mechanistic approach attributed by the hybrid framework as an avant-garde solution in materiobiology and diabetic wound healing nexus. We believe the GQD-hybrid hydrogel reveals an advancement that could portray a new horizon against diabetic wounds.

1. Introduction

Wound healing of diabetic patients could be considered as standing at the eye of the hurricane of a chronic irreparable condition leading to the drastic measure of amputation. Estimations indicate ~70 % of limb amputations are accounted to be as a result of diabetic wounds, which astonishingly suggests with every half a minute that passes, a leg gets amputated globally. [1] Diabetes has been declared a worldwide complex metabolic disorder affecting a population >340 million in number, wherein roughly 20 % of the lot are burdened with diabetic wounds. [2] Although, cognizance into the depressed wound healing of diabetic patients is still obscure; nevertheless, it has been identified that the diminutive glucose metabolization capacity of diabetics traversing to hyperglycaemia extends the wound remediation complexities. [3] Additionally, chronic phases of diabetic wounds are seen to predominantly hamper the healing process vis-à-vis wound hypoxia, and bacterial contamination at the site of wound. [4,5] Hence, diabetic wound dressing is of significance value in the clinical practice, which comes with major shortcomings in terms of bleeding, duration of healing, regenerative ability of bruised tissues, scar development, and jeopardy of sepsis. [6] Along those lines, the complexity of regeneration is supplemented with growth factors, cells, mediators, and cytokines, [7] which follows the hierarchy of phases: hemostasis, inflammation, proliferation, and tissue remodelling. [8] Another important criterion to effective wound therapy is the presence of a moist ambience to promote cell migration, restrict dehydration, and thereby induce accelerated angiogenesis, as well as collagen creation. [9,10]

* Corresponding author at: Amity Institute of Click Chemistry Research and Studies, Amity University, Noida, Uttar Pradesh 201313, India.
** Co-Corresponding author at: Amity Institute of Pharmacy, Amity University, Gurugram, Haryana
E-mail addresses: akumar10@ggn.amity.edu (A.K. Sharma), mmukherjee@amity.edu (M. Mukherjee).
[1] These authors contributed equally as first author.

https://doi.org/10.1016/j.bioadv.2023.213395
Received 29 December 2022; Received in revised form 4 March 2023; Accepted 16 March 2023

Correspondingly, biomimetic hydrogel scaffolds cater to human soft tissues owing to their innate porous system, possessing excellent water-retainability, and wound fluid absorption, while being flexible, henceforth have been explored in biomedical applications viz. wound healing therapies as well as drug vehicles. [11–27] Moreover, it features exceedingly biocompatible characteristic, which could be non-biodegradable and biodegradable solid conformations to render a physical interface for the adsorption and immobilization of biomolecules, viz. growth factors, proteins, along with similar biologically active biomaterials. [28–31] Thence, a plethora of research has been conducted in the myriad of materiobiological applications such as, tissue engineering, bioimaging, invasive drug deployment, cancer therapy, and so on. [11,32]

Furthermore, another factor that hampers with accelerated wound healing is the inevitable bacterial infection of and around the wounded site, and countering this infection is imperative in the diminution of the cumbersomeness of wound remediation. Likewise, approaches towards anti-oxidant medication enables the production of reactive oxygen species (ROS) to cause DNA denaturation and oxidative stress via penetration/disruption of microbial membrane. [33] As a result, engineering smart hydrogels to encapsulate machines having antibacterial activity could beneficially administer wound therapy and thus enhance tissue reepithelization. In this way, the incorporation of 0-D GQDs possessing highly remarkable redox characteristics demonstrates promising potential in antimicrobial performance, while having no apparent toxicity in contrast to other carbon allotropes. [34] Additionally, GQDs are established to exhibit robust peroxidase-like feature as a result of its tremendous electron mobility characteristics. Although, these properties of GQDs have been majorly exploited in bioimaging and sensing, [35–38] GQDs as a pharmaceutical saviour in wound remedy have been contemporarily realised by biomedical researchers globally, but an avant-garde strategy for diabetic wounds.

In this context, Sun et al. investigated the action of GQDs band-aids possessing peroxidase-like function to be a suitable antibacterial material in wound disinfection. [39] They confirmed the catalytic decomposability of H_2O_2 and its subsequent conversion into ·OH enhances antibacterial profile, with an added advantage of controlling the toxicity of high concentrations of H_2O_2 in wound disinfection. They examined against Gram-negative *Escherichia coli* (*E. coli*) and Gram-positive *Staphylococcus aureus* (*S. aureus*) bacteria. Moreover, Wang and coworkers had an interesting approach of investigating the antibacterial potential of GQDs conjugates by means of photodynamic therapy (PDT). [40] The reported conjugate involved the loading of GQDs and erythromycin (EM) inside hollow mesoporous silica nanoparticle (hMSN). The photodynamic component of the experiment led to the generation of singlet oxygen species ($^1O_2$) on irradiation with commercially available LED lamps to cause disruption of bacterial membrane to facilitate improved antimicrobial performance along with regulatable drug release profile. More recently, Zmejkoski and colleagues for the first time incorporated GQDs in a natural hydrogel derived from bacterial cellulose, which was biocompatible and exhibited bactericidal activity against *Streptococcus agalactiae* (*S. agalactiae)*, *S. aureus*, MRSA, MREC (*E. coli)*, and MRPA (*Pseudomonas aeruginosa*). They confirmed the upregulation of matrix metallopeptidase 9, endothelial nitric oxide synthase, Vimentin gene expression, and vascular endothelial growth factor A in fibroblast to insinuate angiogenesis strongly.

In this study, we successfully incorporated GQDs into synthetically engineered PAA (which is chemically represented in (Scheme 1) to overcome the bottlenecks of hydrogels of natural progeniture, [41] thus creating a hybrid hydrogel for fast-action diabetic wound healing within 13 days. Through simple homopolymerization of acrylic acid and subsequent filling of GQDs at different concentrations, we investigate its wound healing enterprise in diabetic Wistar albino rats and correlated the wound closure with expressions of crucial pro- and anti-inflammatory cytokines, IL-6, TNF-α and IL-10. Subsequently, we postulate the multifaceted mechanisms of the wound remedy on the basis of the examinations conducted to fathom the prominent questions like, what makes the collaboration of 0-D filler in matrix to demonstrate dynamic wound remediation and its individual functionalities? Additionally, what was the role of concentration of GQD fillers in hydrogel matrix? Likewise, what is the synergistic activity of GQD-PAA in diabetic wound healing? Finally, the histological and cytotoxic assays were examined to investigate the holistic diabetic wound healing proficiency of the bioinspired hybrid system.

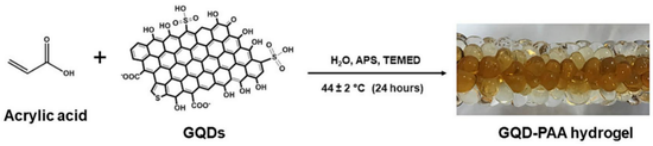

Scheme. 1. Synthesis of GQD-polyacrylic acid hybrid hydrogel.

2. Materials and method

2.1. Synthesis of GQD-PAA hybrid hydrogel

The hybrid hydrogel was fabricated using the mechanism of free aqueous homopolymerization of acrylic acid wherein APS and TEMED were used as accelerator and initiator respectively. Moreover, a slight alteration was carried out in the synthesis technique as previously reported. [42] The process of homopolymerization of acrylic acid was carried out by placing it in a round-bottomed flask under cold temperature conditions, followed by the addition and thorough mixing of distilled water and different concentrations of GQD (0.05 %, 0.1 %, 0.3 %, 0.5 % and 1 %). Following this, nitrogen gas was introduced into the flask for 15 min after which TEMED (0.3 mol%) and concentrated, aqueous solution of APS (0.025 mol% of total monomer concentration) were also added into the flask and the reaction mixture was then mixed perpetually over a magnetic stirrer. Next, after 5 min, the whole mixture was passed into 3 mL test-tubes for the formation of tube-shaped hydrogel. Following this, the mould was dipped up to the height of reaction mixture and positioned vertically upright in a water bath set at a temperature of 44 °C ± 2 °C. Finally, after 24 h, the GQD hybrid hydrogel was cut into small pieces after being detached from the mould. This was followed by its thorough regular washing, removal of unreacted residues by changing of the distilled water for a period of 3 days and finally drying it in hot air oven.

2.2. Chemical characterization

FTIR spectra were performed on ATR-FTIR model, Nicolet-5DX FTIR spectroscopy equipped with a temperature controller using KBr pellets. The measurements were recorded in the wavenumber range of 4000–400 cm^{-1} at a fixed resolution of 4 cm^{-1}. Raman spectra were recorded using Raman Spectrometer connected with a Microscope (Varian 7000 FT-Raman and Varian 600 UMA) and a laser beam of 632.8 nm. X-ray Photoelectron Spectroscopy (XPS) measurements were performed on a Kratos Axis Ultra Photoelectron Spectrometer which uses Al Ka (1253.6 eV) X-rays. Curve fitting and background subtraction were performed using Origin software.

2.3. Morphological characterization

The PANalytical Empyrean X-ray diffractometer was used to get the high-resolution X-ray diffraction (XRD) pattern in the 2θ range of 10° to 80°. Cu Kα radiation (1.5406) was used to record the PXRD pattern. Solid samples that were finely ground were used for Transmission Electron Microscopy (TEM), images were taken on a JEOL, JEM-2100F electron microscope at an acceleration voltage of 200 kV. Samples were

prepared by drop casting the material onto a carbon coated copper grid and then left for drying at room temperature. For pore size analysis, the samples were first swollen in phosphate buffer solutions (PBS) of pH 7.4 followed by freezing in −20 °C for 24 h and then lyophilisation in freeze drier (Ilshin Lab., Co., Ltd., Korea) for 48 h. The morphology of GQD-PAA hydrogels were examined by using Scanning Electron Microscopy (SEM; ZEISS EVO 50). For SEM analysis, the samples were fixed on aluminium stub by using double-sided adhesive conducting carbon tape and were gold coated in a sputter coater (PolaronE 5100 Gold Sputter Coating unit).

2.4. Rheological studies

The rheological investigations were conducted abetted by small-amplitude oscillatory shear experiments on maintaining a fixed stress of 1.0 Pa, on an AR 500 rheometer (TA Instruments, Surrey, England). The cone−plate geometry (2°) was exploited to perform the measurements and silicone oil as well as wet sponges were used to play the role of solvent trap. The storage (G′) and loss modulus (G″) studies in response to frequency were conducted at room temperature. Furthermore, the ratio of G″ to G′ (tan δ) corresponds to the ratio of dissipated energy to the stored energy in one deformation cycle.

2.5. Cytotoxic studies

The cytotoxicity and biocompatibility of hydrogels was assessed on human dermal fibroblast alpha cells (HDF α) by MTT assay. HDF α cells were routinely cultured in Dulbecco modified Eagle medium (DMEM-Himedia) supplemented with 10 % fetal bovine serum (FBS-Gibco), 100 IU/mL penicillin and 100 g/mL streptomycin (Himedia). Cells were maintained at 37 °C with 5 % CO2 in a humidified (humidity-95 %) CO2 incubator (Thermo Scientific).

The different concentrations of GQD-PAA hybrid hydrogels were sterilised by exposing to ultraviolet light for 30 min. Following this, the hydrogels were kept overnight in 10 mL of serum free DMEM in 100 mm petri dishes at 37 °C in a CO2 incubator. After 24 h, the swollen hydrogels were carefully removed using a sterile forceps and the remaining solution was filter sterilised with a 0.22 μm syringe filter. The extracts were further diluted in serum free DMEM (1:3), and assessed for their biocompatibility on HDF α cells.

For MTT assay, the HDF α cells were seeded at a density of 5×10^3 cells per well in a 96 well-flat-bottomed plate (Thermo Scientific) in 200 μL of complete media as described above. Next day, when the cells were attached, the media from the wells was aspirated and the cells were incubated with the extract solutions of hydrogels in CO_2 incubator overnight. Cells incubated with only DMEM were taken as control. The next day, extract solutions were removed from the wells, and MTT reagent {3-(4, 5-dimethylthiazol-2-yl)-2, 5-diphenyl tetrazolium bromide} (Himedia) was added to each well at a final concentration of 0.5 mg/mL in DMEM. After 3 h of incubation, 90 μL of the media was aspirated to remove any unbound MTT and 50 μL of DMSO was added to dissolve the formazan precipitate. The plate was then kept on a shaker for 10 min at 37 °C and absorbance value was recorded at 570 nm on a plate reader.

2.6. In-vitro toxicological analysis

2.6.1. Haemolytic assay

Biocompatibility of any synthesized chemical must be performed to evaluate the toxic and safety profile. Haemolytic rate of any test material indicates the noxious impression compared to Triton X which was taken to achieve complete haemolysis yielding 100 %. Fresh blood was collected and processed for centrifugation at 7000 rpm for 10 mins. The supernatant was discarded, and pellets (having RBC) were washed by PBS (pH 7.4) three times. The initial volume was attained by resuspended in equal amount of buffer solution. This RBC suspension (300 μL) were again mix with 700 μL buffer and test formulation. The mixture was incubated for 1 h at 37 °C and the absorbance was taken at 450 nm for calculating RBC lysis. PBS and Triton X were considered as negative and positive control, respectively. All sample were performed in triplicate mode. The % rate of haemolysis was calculated as:

$$\text{Hemolysis rate\%} = \frac{((\text{sample absorbance}) - (\text{negative control absorban}}{((\text{positive control absorbance}) - (\text{negative control abso}}$$

2.6.2. Hemagglutinin assay

Fresh blood was collected and incubate in 4.9 % citrate phosphate dextrose adenine (CPDA) solution. The mixture was centrifuged at 7000 rpm for 10 mins. The pallet was collected and re-suspended in normal saline (ratio of 1: 9 *v*/v). The resuspended solution (100 mL) was mixed with 600 mL of normal saline and exposed with different formulation respectively. The mixture was incubated for 2 h in 5 % CO_2 incubator at 37 °C and 95 % humidity. After incubation, the mixture of different formulations was smeared on a glass slide and observed under compound microscope at 100×.

2.7. Antibacterial assay

The agar well diffusion method was used to assess the antibacterial activity of the GQD-PAA hydrogels against gram negative *E. coli* (MTCC 1302) bacterial strain purchased from CSIR-IMTech, Chandigarh, India. A layer of autoclaved nutrient agar was poured to the sterile Petri plates, and after it had dried up, 100 μL of bacterial culture with a concentration of 10^7 cells/mL was spread evenly using a cotton swab. The agar layer was then punctured with a sterilised cork-borer and swollen discs of 0.05 % GQD-PAA, 0.1 % GQD-PAA and PAA hydrogels were positioned in the wells to gauge the samples' capacity to kill bacteria. The agar plates were incubated for 16 h at 37 °C. After the incubation period, the inhibition of bacterial growth was examined visually, and the width of the inhibition zone was determined.

2.8. Wound healing assay

2.8.1. Experimental design

Prior to their application, all hydrogels were washed in MiliQ for 3 days for removal of any toxic or unreacted chemicals. Post washing, they were autoclaved and were then used for further experiments. Promoting wound healing was the primary focus of our efforts, we decided to use a sterile powder extract in slurry form. Powder creates a larger surface area, which helps the wound to swell more quickly, provides an immediate hemostatic effect, and speeds up the healing process. The healing process was carried out normally in the control group. The treatment group received a topical application of nanocomposites (0.5 mg) swollen in normal saline (1 mL), and it were applied daily over a circular area that was 10 mm in diameter. The standard group was treated with betadine ointment.

After trimming the hair on the dorsal region of each animal and rinsing it with 10 % povidone and iodine, the area was then disinfected with 70 % isopropyl alcohol. Animals were rendered unconscious through the administration of xylazine (10 mg/kg) and ketamine hydrochloride (25 mg/kg) via intraperitoneal injection. A biopsy punch with a diameter of 10 mm (manufactured by Accuderm in the United States) was used to create a full thickness excisional wound.

In the excision wound model, wound area was measured by tracing the wound with the help of a transparent sheet using millimeter-based graph paper at different time points for each group. This was done at various points throughout the experiment. The contraction of the wound was measured using following formula:

$$\text{Wound closure } (\%) = \frac{(\text{Initial Wound Area}) - (\text{Specific Day Wound Area})}{\text{Initail Wound Area}}$$

2.8.2. Assessment and analysis of various pro-inflammatory and anti-inflammatory cytokines

Pro-inflammatory (IL-6, TNF-α) and anti-inflammatory (IL-10) cytokine levels were investigated at the site of excisional wound in normal and drug-treated animals on 4th and 13th day. An enzyme-linked immunosorbent assay was used to calculate the level of inflammatory cytokines in the serum sample obtained from the blood sample of animals of diverse groups (sandwiched ELISA kit, Ray Biotech, USA) (17). The assays were performed according to the manufacturer's instructions wherein first, the washing of wells was performed followed by the biotinylation of the different antibodies (IL-10, IL-6 and TNF-α). Thereafter, the unbound or excess biotinylated antibody was removed by washing, following which HRP-conjugated streptavidin was further added. The wells were rinsed followed by the addition of TMB substrate and absorbance of the sample was at 450 nm.

2.8.3. In-vivo toxicological analysis

2.8.3.1. Histological assessment of vital organs and wound area. All animals were sacrificed at the end of experiment protocol. In-addition to skin sample of wound area, the vital organs including brain, heart, liver, and kidney were dissected immediately after scarification of animals. The isolated organs were washed with normal saline and stored in 10 % formalin solution (pH 7). The tissue was dehydrated by immersing in ascending grades of ethyl alcohol, clearing by absolute xylene, and impregnated with molten paraffin wax. The paraffin blocks of embedded tissue were sectioned with Rotary Microtome at 5–6 μ thickness. The tissue sections were incubated for deparaffinization and stained with haematoxylin and eosin. The microscopic slides of stained sections were examined under light microscopy (100×).

2.8.3.2. Statistical analysis. Biochemical assessment of different parameters as compared to control group was assessed by statistical analysis using one-way analysis of variance (ANOVA) followed by Tukey's test. All data were expressed as mean ± standard deviation (SD) and the *p* value was calculated. A p value < 0.05 was considered as statistically significant.

3. Results and discussions

3.1. Chemical and morphological characterization of GQD-PAA hybrid hydrogel

The orientation of polymeric chain and fillers in GQD-PAA hybrid hydrogel can be predicted by investigating X-ray diffraction pattern (Fig. S2). Wide angle X-ray study and small angle X-ray study are used to determine the change in crystallinity and the extent of filler dispersion. [43] In XRD graph, the GQD-PAA hybrid hydrogel shows a broad peak of 2θ value of 20° indicating semi-crystalline nature and random network formation in hydrogel. Absence of a 2θ peak at 27° in GQD-PAA hydrogel indicates formation of a highly oriented structure owing to Van Der Waals interaction between GQD and acrylic acid.

The interactions of PAA polymer with GQDs have been analysed abetted using FT-IR spectroscopy, is depicted in Fig. 1a. IR spectra of PAA shows very broad band at 3450 cm^{-1}, characteristic of the stretching OH vibration of carboxylic group and a peak at 2925 cm^{-1} corresponds to C—H stretching of methyl group. Further, a peak at 1715 cm^{-1} denotes CO stretching vibration and a peak at 1450 cm^{-1} pertains to C—H bending vibration. However, fingerprint region 1350–730 cm^{-1} corresponds to in-plane and out-of-plane bending vibration of OH and C—H. While the hybrid GQD-PAA FT-IR spectra shows OH stretching peaks at 3558 cm^{-1} and 3589 cm^{-1} which represent the presence of chemically different alcoholic/phenolic groups with varying binding strengths and force constants in the molecule. A weakened vibration peak at 2925 cm^{-1} corresponds to C—H stretching of methyl group and a peak at 1715 cm^{-1} pertains to C=O stretching. Distinct, peak at 803 cm^{-1} in the GQD-PAA spectra corresponds to C—S stretching and peak at 1163 cm^{-1} corresponds to symmetric stretching vibration of $S(=O)_2$ group present at edges of GQDs.

Raman spectroscopy is a crucial non-destructive method for identifying many sorts of defects in carbon materials, such as grain boundaries, point defects, stress, strain, stacking faults, edges, doping, vacancies, functional groups, etc. A typical Raman spectrum of GQD-PAA hydrogel is shown in Fig. 1b, representing a weaker D band at 1359 cm-1 and a strong G band at 1579 cm. The disorder created by increase in size is associated to the D band, whereas the in-plane vibration of the sp^2 carbon atoms is related to the G band. The I_D/ I_G ratio of pure GQD is 1, [44] while the measured I_D/ I_G ratio of the synthesized GQD-PAA is 0.78, decrease in I_D/ I_G ratio serves as a gauge for the flaws that has developed due to the interaction of GQD with the hydrogel matrix.

To study the chemical-bonding state of synthesized hybrid 0.1 % GQD-PAA hydrogel, XPS measurements were performed to determine the composition in accordance to quantitatively analyse the hybrid framework. The binding peaks (Fig. 1c) at 284 eV and 531.3 eV are ascribed to C1s and O1s electrons, and a small peak at 166.8 eV for the S2p electrons which are the crucial elements of GQD-PAA hybrid hydrogel. The deconvolution of the C1s, O1s, and S2p peaks into four, three and three Gaussian components, respectively, allowed us to examine the configurations of the carbon, oxygen and sulphur atoms in GQD-PAA hybrid hydrogel. The C1s spectrum (Fig. 1e) was deconvoluted into two large and two small peaks centred at 283 eV (for C=C), 285 eV (for C—C, C—H), 287.1 eV (C-OH, C—S, C-O-C), 289.4 eV (COOH, C=O). The O1s spectrum (Fig. 1d) was deconvoluted into one large and two relatively smaller peaks centred at 531.4 eV, 532.4 eV and 534.1 eV representing the different forms of oxygen i.e., -OH, C=O/COOH, C—O respectively. The greatest intensity of COOH/C=O implies that the carboxyl group is more exposed at the edge locations of GQD-PAA hybrid hydrogel. The weak peak at 166.8 eV in survey peak confirms the presence very less amount of sulphur in GQD-PAA hydrogel. S2p spectrum (Fig. 1f) was deconvoluted into three peaks centred at 168.8 eV (for S—O) and 163.1 eV (for C—S) showing the presence of sulphur in two forms, and peak at163.2 eV (for $2p_{3/2}$) represents thiophene like S peak due to spin orbit coupling.

Surface morphological of GQD-PAA hydrogel have been evidenced using SEM. The narration of the SEM images has been organized to depict post swelling conditions in acidic pH 1.2 (Fig. 2a and b), wherein GQD-PAA hydrogels are seen to be comparatively non-porous owing to the ionisation of PAA units, attributing to a scarcely porous framework. Subsequently, at pH 7.4 (Fig. 2e-g) GQD-PAA develop into macroporous structures, with an average PAA hydrogel pore size of ~46 μm. Interestingly, the average pore size was observed to ameliorate to ~120 μm in the GQD-PAA hybrid hydrogel network. The ionisation (deprotonation) of the AAc units (-COO) was identified to be the primary cause of swelling. Furthermore, the equilibrium swelling ratio (ESR) corroborates with the evidences from SEM (Fig. S3). Moreover, the ionisation of the pendant groups influences the PAAc chains to split, and the resulting electrostatic repulsion accommodate the network to enlarge for the percolation of water. [45] The amount of water trapped within the polymeric skeleton is directly proportional to size of pore created during lyophilisation. Conversely, the external surface morphology of hydrogel was unlike the interior (Fig. 2d), with the walls encircling the gel represented an impermeable continuous outer skin, whereas the internal surface revealed a hollow porous interconnected honeycomb like conformation. In Fig. 2h-i, wrinkles are observed in GQD hybrid hydrogel depicting distinctive corrugation that resembles crumpled GQD. The prominence of wrinkles was seen to be enhanced with augmentation in GQD concentrations. At its most concentrative,

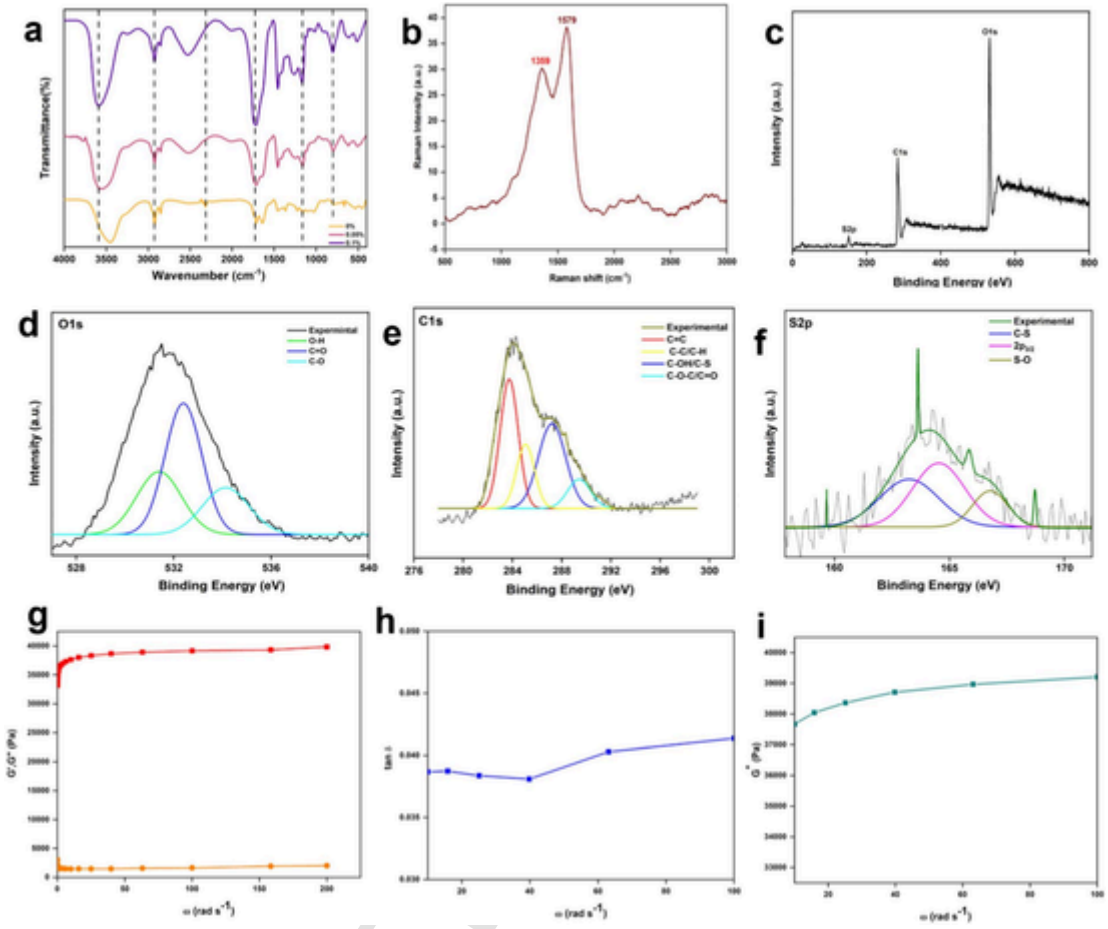

Fig. 1. Represents (a) FTIR spectra of 0 %, 0.05 %, and 0.1 % of GQD-PAA hybrid hydrogel, (b) Raman spectra of 0.1 % GQD-PAA hydrogel, and XPS peak of 0.1 % GQD-PAA hydrogel composite, (c) survey peak, (d) O1s peak, (e) C1s peak, (f) S2p peak. Rheology studies of 0.1 % GQD-PAA hybrid hydrogel represents frequency dependence of viscoelastic characteristics apropos (g) storage (G′) and loss modulus (G″) studies in response to frequency, (h) loss factor (tan δ), and (i) complex modulus.

GQDs aggregate to develop into sheet-buckles, producing tubular or fibril structures.

The incorporation of GQD machines into PAA hydrogel nanotube (HNT)-like matrix were visualised through TEM, along with the estimated d-spacing of ~0.23 nm. Revelations from this highly sophisticated microscopic instrument identified the GQDs to uniformly organized in the matrix at low filler percentages (Fig. 2j), however, the amelioration of GQD incorporation percentage induced a robust interaction of GQDs with the innate functional groups of the HNTs. It was reconnoitred that the formation of HNT-like morphologies were created as a result of preferential stacking and rolling of sheets (Fig. 2 k-l) in an explicit direction during polymerization. [46] This was accounted to be governed by the temperature, which was seen to be the protagonist in influencing the buckling of polymer nanosheets into hollow nanotubes (Fig. 2 m-p) with a seamless pattern reminiscent of the art of origami. [47] This curvature-induced strain imposes a transverse gradient of stress that rolls the stacked sheets concentrically directed by van der Waals interactions with a hollow internal cylindrical conduit, which provides a novel route for polymer confinement controlled by polymer chain dynamics.

3.2. Cytotoxic studies

The various concentrations of GQD-PAA hydrogels were tested on its biocompatibility in-vitro using the MTT assay, which is portrayed in Fig. S5. We employed human dermal fibroblast alpha cells (HDF α cells) to perform this examination, which were primarily obtained from human skin tissue. Hydrogel-incubated culture medium exhibited no substantial toxicity to HDF α cells. All hydrogel extracts demonstrate HDF α vitality >84 %; however (Fig. S5a3-5), 0.05 % GQD-PAA and 0.1 % GQD-PAA hybrid hydrogels showed cell viabilities of >90 % and > 95 % (Fig. S5a1-2), respectively, when compared to merely the DMEM control group (100 %) (Figure S5acontrol). Most importantly, our findings indicate that these two samples hold immaculate potential to be employed as hydrogel based wound dressings in the near future.

3.3. In-vivo toxicological examinations

3.3.1. Effect of GQD-PAA formulation on RBC haemolysis

Assessment of RBC haemolysis was performed to analyses toxicological impact of various GQD-PAA based formulation. Fresh blood sample was exposed to PBS and Triton X sample. The percentage haemolysis was measured after 1 h incubation. Haemolytic rate of different formulations was seen to be less than permissible rate which showed no toxic effect of numerous formulations as compared to triton X and normal control. Interestingly, the % haemolysis of GQD-PAA (0.05) and GQD-PAA (0.1) was comparative lowered than other formulations which indicate their high safety margin or less toxicological impact, which can be seen in Fig. S6a.

3.3.2. Effect of GQD-PAA formulation on RBC agglutination

RBC agglutination is another in-vitro assessment assay for measuring the biocompatibility of test sample has been depicted in Fig. S6b.

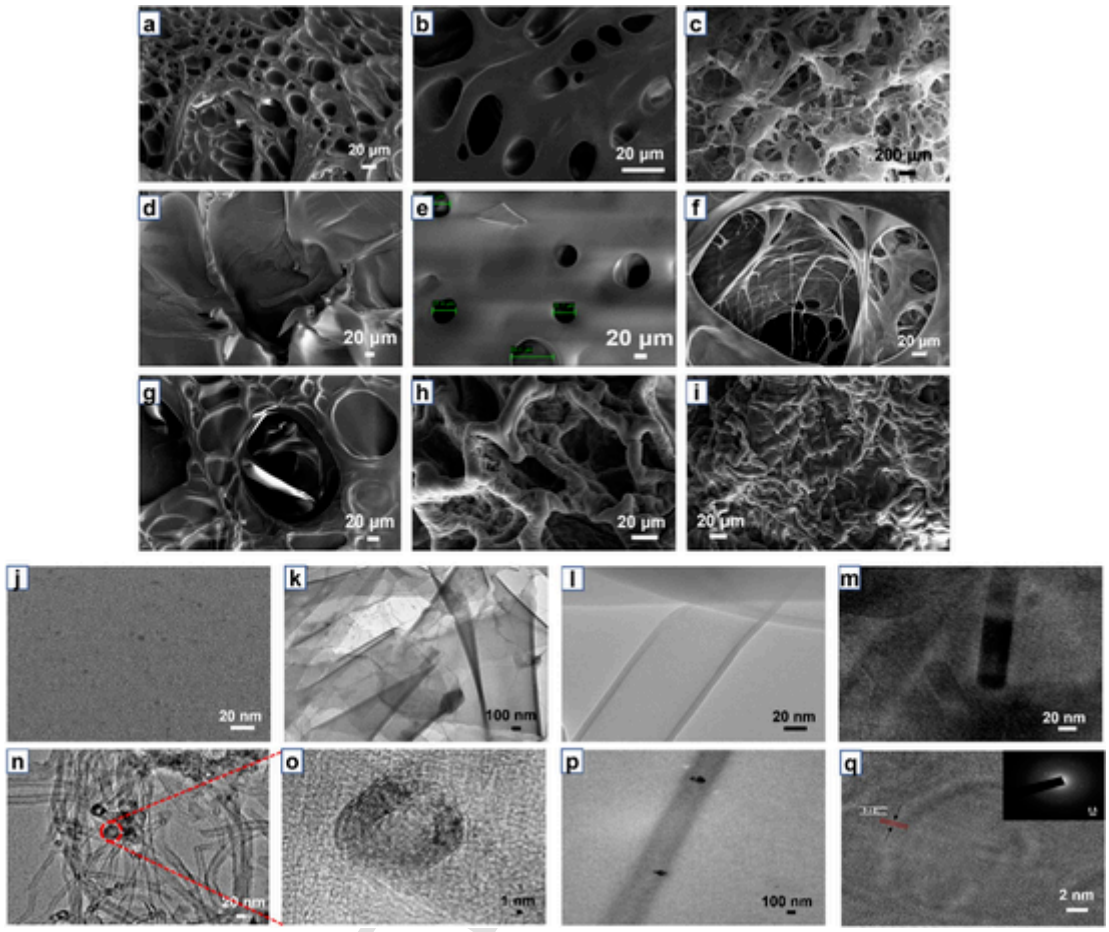

Fig. 2. SEM micrographs of swollen GQD-PAA hydrogels: (a-c) cross-section after swelling in pH 1.2 and 7.2 respectively; (d) external surface of hydrogel after swelling in PBS (pH 7.4); (e-g) average pore size of PAA hydrogel and GQD-PAA respectively; (h-i) polymer wrinkles. TEM micrograph of GQD-PAA hydrogel: (j) showing distribution of GQD in hydrogel matrix. (k-l) stacking and rolling of polymer sheet. (m-n) tubular architecture, (o) enlarge tubular architecture. (p) impregnated GQD within nanotube. (q) SAED pattern corresponds to area in image (Inset: SAED pattern).

The consequences of hemocompatibility assay showed no or negligible RBC aggregation in GQD-PAA formulation treated samples and found to be comparable with normal control (PBS) slide. The observation suggests the biocompatibility of different formulations of GQD-PAA, and individual treatment of GQD and PAA.

3.4. *In-vivo toxicological investigations*

3.4.1. *Effect of GQD-PAA formulation on histology of vital organs*

Scientific tactic towards the safety and effectiveness of synthesized material in managing the diverse ailments suggest to evaluation of in-vivo toxicity emphasizing vital organs. Toxicological assessment is the crucial method for determining the adverse effects of selected formulation in animal model, which could extrapolate to predict the toxicity or safety profile in humans. Histological assessment of vital organs was performed for evaluation of in-vivo toxicity of different formulations applied during wound healing treatment. Although it is not common to produce significant systemic and vital organ toxicity by topical formulations, but reports suggest systemic absorption of hazards molecule can potentially lead to failure of vital organs. Thus, for better validation we evaluated the effect of GQD-PAA formulations on structural arrangement of vital organs. Histological analysis of hepatic tissue, cardiac tissue, brain tissue and renal tissue were carried for finding the presence of central vein and normal hepatic cord (in liver tissue), normal nuclei, muscle fibres, and intercalated disc (in heart tissue), hippocampus (CA1) region, normal granular cell of dentate gyrus and glial cells (in brain tissue) and glomerulus, renal tubules, and blood vessels (in kidney tissue). Photomicrographs of these vital tissue of animals treated with 0.05 and 0.1 % GQD-PAA hybrid hydrogel in Fig. 3 showed insignificant or no structural alteration in the GQD-PAA treated animals at any concentrations as compared to normal control. The histological outcomes indicate no toxicological impact of GQD-PAA formulations with any concentration and individual treatment of GQD and PAA that support the in-vitro results of safety profile, as seen in Fig. S7.

3.5. *Effect of GQD-PAA hybrid hydrogels on wound healing rate*

The wound contraction rate in diabetic rats of each group was assessed for 13 days in response to the respective therapeutic interventions on the wound surface, which is depicted in Fig. 4. The percentage wound contraction was evaluated for daily treatment of varied concentrations of GQD-PAA, standard and normal control. Initially, it was observed that the rate of wound closure was slow in all groups barring 0.05 % GQD-PAA hydrogel, which was complimented with a significant jump on 4th day recording a wound closure rate of 16 %, as compared to the standard, which only exhibited 10 % wound closure rate. Likewise, a substantial improvement in the wound closure rate was observed with 0.1 % GQD-PAA hybrid hydrogel on the 4th day, with a dramatic elevation from 1 % to 10 %, contrastingly to the normal control group having wound closure rate of only 7 %. Moreover from 9th to 13th day, a continuous and consistent enhancement in wound closure rate was observed in 0.05 % and 0.1 % GQD-PAA hybrid hydrogel treated animals as compared to all other groups. Complete healing

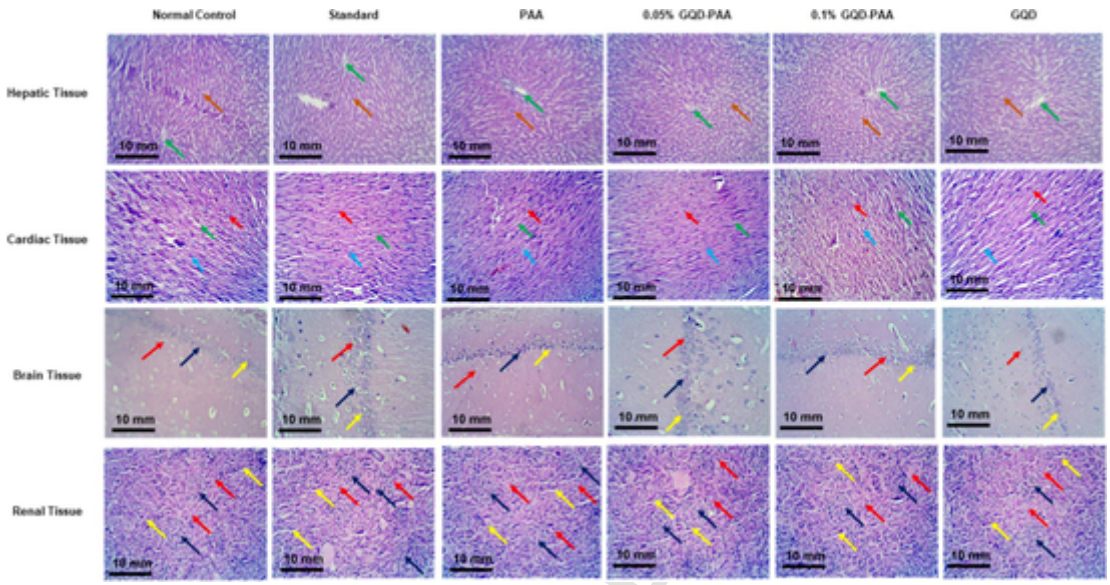

Fig. 3. Histological assessment of hepatic and cardiac tissue of animals treated with normal control, standard and various formulation of GQD-PAA based on different concentrations. Green arrow showed central vein and brown arrow represent hepatic cord in H&*E*-stained hepatic tissues. Red arrow showed normal nuclei, blue arrow present muscle fibre and green arrow indicates intercalated disc in H&E-stained cardiac tissue at magnification of 100×. Histological assessment of brain and renal tissue of animals treated with normal control, standard and various formulation of GQD-PAA based on different concentrations. Blue arrow showed Hippocampus (CA1) region, red arrow present Normal granule cell of dentate gyrus and yellow arrow represent glial cells in H&E-stained brain tissues. Blue arrow showed normal glomerulus, red arrow present normal renal tubules and yellow arrow indicates renal blood vessels in H&E-stained kidney section at magnification of 100×. (For interpretation of the references to colour in this figure legend, the reader is referred to the web version of this article.)

(wound closure rate = 100 %) was observed in the diabetic wounds administered with 0.05–0.1 % GQD-PAA hybrid hydrogel on the 13th day (indicative of accelerated wound healing) as compared to the normal control and standard. Conclusively, it could be inferred that particularly 0.05 % and 0.1 % could produce accelerated wound healing in correspondence to the improved cellular proliferation and migration of epithelial cells to the site of trauma. These treatments also expedite the rate of re-epithelialization in wound-healing process in comparison to the normal control and standard groups, thus demonstrating a dominating modification of cellular events. Eventually, by the 16th day all the different concentrations of GQD-PAA hybrid hydrogels could induce effective wound healing but at diverse rates that showed promising consequences of diabetic wound healing potential of this hybrid hydrogel. Moreover, diabetic wound closure by other filler concentrations of the hybrid hydrogels is represented in Fig. S8.

The assessment of numerous structural changes near the excision line of wound corresponding to the healing status of injured tissue has been represented in Fig. 4. The deposition of polymorphonuclear leucocytes (PMNL) formation of collagen and reepithelization across the wound area was assessed by semi-quantitative evaluation method. The presence of PMNL cells or inflammatory cells adjacent to the excision line of wound is indicated by leukocytes infiltration. Moreover, the exudate (necrotic cells) formation can be identified by demarcation line around the wound area which also represents the accumulation foreign substance. Exudate accumulation and high leukocytes infiltration or accumulation of PMNL cells restrict the healing rate of wound. The treatment of different formulations of GQD-PAA significantly reduced the leukocytes infiltration/inflammatory cells and exudate formation near the excisional line as compared to normal control group that indicates their ability to accelerate the wound healing rate. Photomicrograph also shown the angiogenesis in GQD-PAA treated animal's tissue. Angiogenesis reflects the growth of new blood vessels from the existing vasculature that allow increased supply of oxygen and nutrients which support the healing of wound. Additionally, the accumulation of collagen around the excisional line reflects the healing process of surrounding cell which tend to upsurge the strengthening between damaged and nearby cells to uplift the wound healing. Furthermore, the re-epithelization of injured tissue indicates the formation of new dermal layer and achieved at the final phase of wound healing. The histological analysis of skin tissue of respective group having treatment of different GQD-PAA formulations showed the upsurged collagen deposition and re-epithelization and indicate the healing ability as compared to normal control animals. Interestingly, on comparing the collective consequences of tissue histology we found that GQD-PAA (0.05) and GQD-PAA (0.1) showed and lowest level of leukocytes infiltration, significant lack of exudate accumulation, collagen deposition, presence of angiogenesis and complete re-epithelization as compared to other formulations. These ameliorated structural changes in GQD-PAA (0.05) and GQD-PAA (0.1) treated group indicates its significant potential to accelerate wound healing rate. The results of higher filler concentrations of the hybrid hydrogels are depicted in Fig. S8.

3.6. *Effect of GQD-PAA hybrid hydrogels on inflammatory cytokines*

The process of wound healing comprises of the release of both pro-inflammatory (IL-6, TNF-α) and anti-inflammatory (IL-10) cytokines. In physiological process of wound healing, the release of inflammatory cytokines plays an important role to regulate the incidence of pain and inflammation. The release of these inflammatory cytokines is an integral mechanism of body homeostasis during healing of internal or external injury. To corroborate the statements pro and anti-inflammatory cytokine were accessed on early and lateral stage of wound healing. In the initial phases of wound healing, inflammation occurs because of pro-inflammatory cytokines, which facilitates the formation of blood clot, permeation of blood vessels, and migration of leukocytes and neutrophils. However, prolonged release of pro-inflammatory cytokines may lead to delayed wound healing. Correspondingly, it can be noticed that IL-6 and TNF-α to be highly expressed in all the cases on day 4, however it is noteworthy to mention that lower filling percentages of GQDs (0.05 and 0.1 % GQD-PAA) demonstrate contrastingly lower concentrations of expressions on day 4 as well as day 13. On quantifying the results, of 0.05 % and 0.1 % GQD-PAA hybrid hydrogel, the value

of IL-6 stood at approximately 580 pg/mL, as compared to normal control and standard (680 pg/mL and 630 pg/mL respectively), as seen in Fig. 5a. Similarly, the treatment of 0.05 % and 0.1 % formulations significantly reduced TNF-α level (540 pg/mL) as compared to normal control and standard groups (660 pg/mL and 600 pg/mL respectively), as represented in Fig. 5b. Whereas the value of IL-10 was found moderately higher (450 pg/mL) than normal control and standard treatment groups (340 pg/mL and 370 pg/mL respectively), as represented in Fig. 5c. Conversely, the lateral phase of wound healing, where the wound has relatively less microbial invasion, the inflammatory response gradually declines by increased release of anti-inflammatory cytokines which further promote cell proliferation and migration, angiogenesis, and synthesis of extracellular matrix. Subsequently, studying IL-10 expression elucidates highest expression in 0.05 and 0.1 % GQD-PAA hydrogel composites, which corroborates well to confirm its efficacy as a promising tissue regeneration scaffold in wound dressing application. The availability of high concentration of released IL-10 at lateral stage (13th day) of wound healing by the application of different formulations of GQD-PAA hybrid hydrogel revealed their anti-inflammatory potential. Our results showed that application of 0.05 % and 0.1 % GQD-PAA hybrid hydrogel engendered an IL-10 concentration of around 210 pg/ml, as compared to normal control and standard (135 pg/mL and 160 pg/mL respectively). These consequences further endorse the potent anti-inflammatory activity of 0.05 % and 0.1 % GQD-PAA hybrid hydrogel formulation which showed significant rise of IL-10 level in respective treatment group along with immaculate elevation of wound healing rate. Higher filler percentages of GQD-PAA hybrid hydrogel have been illustrated in Fig. S9. In relation to the expression of cytokines, the wound closure rate (%) was statistically evaluated and illustrated in Fig. S10 elucidating the brilliance of 0.05–0.1 % GQD-PAA in treating diabetic wounds.

3.7. Diabetic wound healing mechanism

To provide cognizance over the obtained wound healing in this report in relation to the release of pro- and anti-inflammatory cytokines, we investigated it from a material scientific perspective to identify the role of individual component of the hybrid network and its collaborative activity. Initially, it is imperative to focus on maintaining sufficient oxygen levels, which is crucial in governing neovascularization, cell

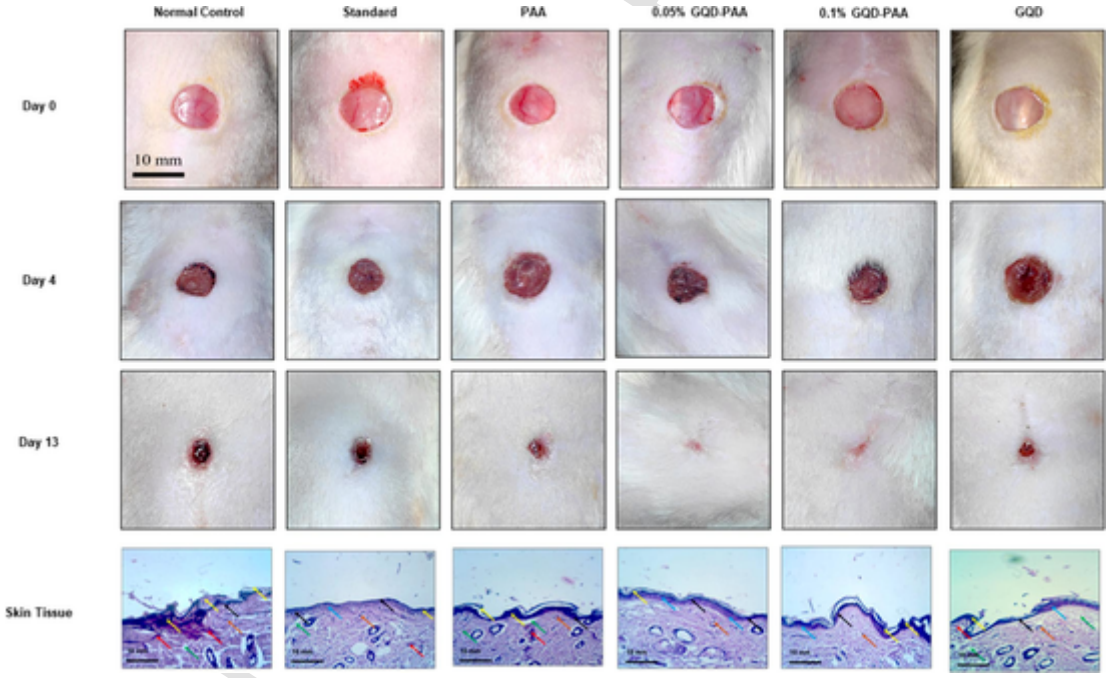

Fig. 4. In vivo wound healing evaluation. Study showing control, standard, and hybrid hydrogel administered to treat diabetic wounds in Wistar rats on days 0, 4th, and 13th days. Figure portrays the histological effect of normal control, standard and various formulation of GQD-PAA based on different concentrations on diabetic wounds. Black arrow showed re-epithelialization, red arrow present leukocytes infiltration, yellow arrow indicates exudates deposition, green arrow showed collagen deposition, brown arrow represents angiogenesis and blue arrow showed tissue granulation in H&*E*-stained skin tissues of wound area at magnification of 100×. (For interpretation of the references to colour in this figure legend, the reader is referred to the web version of this article.)

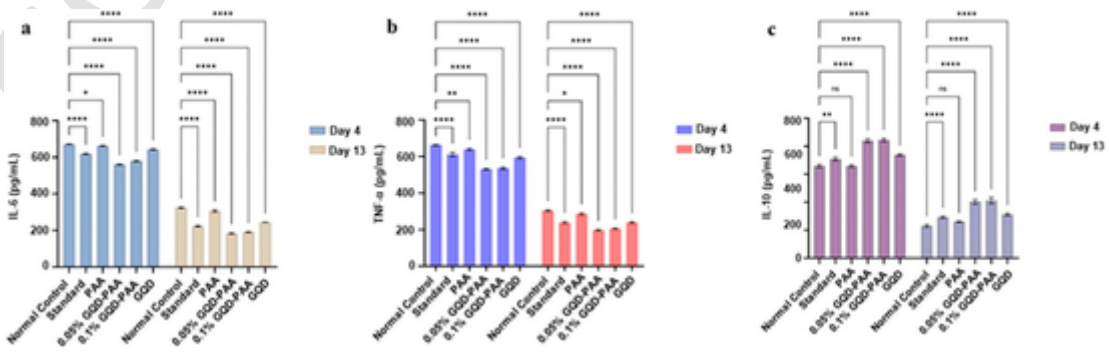

Fig. 5. Quantification of (a) IL-6, (b) TNF-α, (c) IL-10 at days 4th and 13th post-wound closure.

proliferation, and migration to facilitate augmented wound healing. [48–53] Thence, it could be realised from the morphological characterizations (Fig. 2), the porosity of the matrix as well as the crumpled conjugate of GQD-PAA percolates oxygen, thus arresting wound hypoxia by enabling the tissue to respire effectively. [54,55]

Furthermore, the nano-regime of GQDs plausibly encourages enzymatic functions viz. oxidase, which is accountable to catalyse oxidation-reduction reaction, thus leading to generation of reactive oxygen species (ROSs), to functionally kill diabetic wound-related bacteria by means of cell membrane disruption triggered by hyper lipid peroxidation, thereby damaging microbial DNA and proteins. [56,57] Likewise, Zhong et al. investigated a novel biogenically developed nanocomposite by coating silver nanoparticles (AgNPs) (GQDs@Ag) to expedite the healing of methicillin-resistant *Staphylococcus aureus* (MRSA)-infected wounds. [58] They reported a substantially robust generation ROS as a result of the oxidase-like functionality of the composite, which facilitated the destroying of the bacteria by wounding the bacterial membrane and as a result DNA and protein to cause apoptosis of MRSA. In accordance, we observed an augmentation in the zone-of-inhibition (ZOI) with *E. coli* (Fig. S4) in the following hierarchy: PAA < GQD-PAA (0.05 %) < GQD-PAA (0.1 %), which empirically describes volatile antibacterial characteristics of the designed nexus. Interestingly, in relation to its size, GQDs were also responsible for cell signalling mechanism, which induces immediate inflammation stage of the wound healing through the initial spike of IL-6, [59] as observed above (Fig. 5a). It is noteworthy to mention that the hydrophilicity of the hydrogels is necessary to impart a moist ambience for cells to migrate, consequently influence lucrative cell proliferation and thus wound healing. [60] Correspondingly, the ESR investigations in corroboration with SEM images reveals the GQD-PAA nexus to exhibit excellent swelling performances to enable effective absorption of wound fluid, while maintaining a wet environment for the cells to migrate, and thus expedite the wound healing process (Fig. S3 and Fig. 2e-g). Therefore, in response to the SEM and optical image examination of GQD-PAA hydrogel (Fig. 2h-i and Fig. S1), it can be postulated that the increase in GQD concentrations reduces the available space in the hydrogel for it to create a watery milieu, thus hindering wound remediation in the diabetic rat models. Hence, it is necessary to take appropriate percentage of GQD fillers to carry out wound healing activity without hampering the innate benefits of hydrophilic hydrogel matrix. In relation, we observed a dynamic diabetic wound healing in 0.05–0.1 % GQD-PAA nexus biomimetic scaffold in 13 days.

4. Conclusion

In conclusion, our study explores the nascent possibility of incorporating 0-D GQD fillers into PAA hydrogel matrix to create a hybrid biomimetic scaffold for fast-action diabetic wound healing activity, demonstrating rapid wound closure in 13 days. In this report, we administered various concentrations of GQD-PAA in diabetic Wistar albino rat models to examine its wound healing response. In contrast to natural control and standard betadine, the hybrid hydrogel reported excellent wound remediating activities, specifically we observed lower incorporation percentages of GQDs (0.05–0.1 % GQD-PAA) to exhibit complete wound closure by the 13th day. This result corroborates well with the pro- and anti-inflammatory expression studies, which initially records a spike in IL-6 and TNF-α on day 4, indicating the initiation of inflammation stage of the wound healing process, however it is noteworthy to highlight that the lower concentrations of GQD-PAA exhibited lower pro-inflammatory cytokines in contrast to control, betadine and higher filler percentages of GQD-PAA hydrogel. Contrastingly, the rat models administered with 0.05–0.1 % GQD-PAA hydrogels showed higher IL-10 values as compared to other test samples. The transversion from inflammation phase cell proliferation and angiogenesis was characterized by the gradual decline in the concentrations of pro-inflammatory cytokines, meaning there was no delay in the wound healing process. From these results, we postulated the hydrophilicity in conjugation with the porosity of the hydrogel framework allows for the oxygenation and regulation of a moist milieu for the cells to migrate and thereby heal the wound in a scarless fashion. Along the same lines, the nano-dimension of the filler attributed to the cell signalling pathway necessary to induce initial inflammation as well as plausibly generate ROS to simultaneously destroy the bacterial infection consequences of the diabetic wound. Additionally, it was cognized that the overfilling of GQDs could leave no vacancy for cells to interact with the hydrophilic nature of the hydrogels, and furthermore affect oxygenation by closing the pores, therefore hamper the dynamicity of the wound healing process. Finally, the cytotoxic assays and histological examinations determined the as-prepared hybrid hydrogel with reference to natural and standard control to be substantially biocompatible and effectuate dynamic diabetic wound healing without affecting the healthy cells. The hybrid hydrogels demonstrated to possess antibacterial characteristics, biocompatibility, porosity, water-retainability and wound fluid absorption characteristics. Furthermore, the superiority of synthetic PAA hydrogels compared to natural gels in terms of structural integrity, demonstrates to be a promising band-aid. Owing to the conglomeration with GQDs permits antibacterial and cell-signalling functionality to facilitate expedited angiogenesis and promote wound closure by feeding sufficient oxygen and maintaining a moist environment to influence cell migration lucratively.

Supplementary data to this article can be found online at https://doi.org/10.1016/j.bioadv.2023.213395.

CRediT authorship contribution statement

Kumar Shivam: Synthesized the hydrogels, performed microbial experiments, data analysis and written the manuscript. Abhyavartin Selvam: Material characterization, analysis and written the manuscript. Sujata Sangam: Material characterization, analysis and written the manuscript. Misba Majood: Performed the biological experiments and written the manuscript. Siddhartha Pahari: written the manuscript. Ranjan Patra: Writing- Reviewing and Editing. Arun K Sharma: Performed the in-vivo experiments, writing- reviewing and editing. Monalisa Mukherjee: Supervision, Conceptualization, Methodology, Reviewing and Editing.

Declaration of competing interest

The authors declare that they have no known competing financial interests or personal relationships that could have appeared to influence the work reported in this paper.

Ethical Standards

Male Wistar albino rats weighing 200-220 g were procured from Animal House Facility of Institute of Pharmacy, Amity University, Noida, India approved by the 'Institutional Animal Ethics Committee'. All animals were acclimatized first in 'Institutional animal house' on the basis of accepted protocol of Committee for the Purpose of Control And Supervision of Experiments on Animals (CPCSEA) New Delhi, India, and utilized for the present investigation. Throughout the study, the animals were accommodated in independent cages and perpetuated normal ambient conditions (temperature 20 ± 2 °C, relative humidity 60 ± 10 %). All rat models were provided access to normal water and food ad libitum.

Data availability

Data will be made available on request.

Acknowledgements

Monalisa Mukherjee thanks the Department of Biotechnology (DBT) BT/PR21866/NNT/28/1145/2016 and Department of Science and Technology (DST), Science and Engineering Research Board (SERB) (EMR/2016/00561) for funding this project, and Amity University Uttar Pradesh (AUUP) Noida for providing research infrastructure. The group is thankful to Maryam Ghufran for helping with the cytotoxicity study and Dr. Puja Prasad for valuable comments. The authors would like to acknowledge the biorender software for figures.

References

[1] V. Vijayakumar, S.K. Samal, S. Mohanty, S.K. Nayak, Recent advancements in biopolymer and metal nanoparticle-based materials in diabetic wound healing management, Int. J. Biol. Macromol. 122 (2019) 137–148, https://doi.org/10.1016/J.IJBIOMAC.2018.10.120.

[2] A. Nicolucci, Fact and figures about diabetes in Italy, Assist. Inferm. Ric. 30 (2011) 100–106, https://doi.org/10.1702/845.9396.

[3] S. Patel, S. Srivastava, M.R. Singh, D. Singh, Mechanistic insight into diabetic wounds: pathogenesis, molecular targets and treatment strategies to pace wound healing, Biomed. Pharmacother. 112 (2019) 108615, https://doi.org/10.1016/J.BIOPHA.2019.108615.

[4] S.A. Eming, T.A. Wynn, P. Martin, Inflammation and metabolism in tissue repair and regeneration, Science 356 (2017) (1979) 1026–1030, https://doi.org/10.1126/SCIENCE.AAM7928.

[5] S. Guo, L.A. DiPietro, Factors affecting wound healing, J. Dent. Res. 89 (2010) 219–229, https://doi.org/10.1177/0022034509359125.

[6] S. MacNeil, Progress and opportunities for tissue-engineered skin, Nature 7130 (445) (2007) 874–880 https://doi.org/10.1038/nature05664, 2007 445.

[7] S. Barrientos, H. Brem, O. Stojadinovic, M. Tomic-Canic, Clinical application of growth factors and cytokines in wound healing, Wound Repair Regen. 22 (2014) 569–578, https://doi.org/10.1111/WRR.12205.

[8] B.K. Sun, Z. Siprashvili, P.A. Khavari, Advances in skin grafting and treatment of cutaneous wounds, Science 346 (2014) (1979) 941–945, https://doi.org/10.1126/SCIENCE.1253836.

[9] L. Zhang, M. Liu, Y. Zhang, R. Pei, Recent Progress of highly adhesive hydrogels as wound dressings, Biomacromolecules 21 (2020) 3966–3983, https://doi.org/10.1021/ACS.BIOMAC.0C01069.

[10] Y. Zeng, R. Zou, Y. Zhao, Covalent organic frameworks for CO2 capture, Adv. Mater. 28 (2016) 2855–2873, https://doi.org/10.1002/ADMA.201505004.

[11] A.J.T. Teo, A. Mishra, I. Park, Y.J. Kim, W.T. Park, Y.J. Yoon, Polymeric biomaterials for medical implants and devices, ACS Biomater Sci Eng. 2 (2016) 454–472, https://doi.org/10.1021/ACSBIOMATERIALS.5B00429.

[12] N. Annabi, D. Rana, E. Shirzaei Sani, R. Portillo-Lara, J.L. Gifford, M.M. Fares, S.M. Mithieux, A.S. Weiss, Engineering a sprayable and elastic hydrogel adhesive with antimicrobial properties for wound healing, Biomaterials 139 (2017) 229–243, https://doi.org/10.1016/J.BIOMATERIALS.2017.05.011.

[13] D.Z. Zmejkoski, Z.M. Marković, D.D. Mitić, N.M. Zdravković, N.O. Kozyrovska, N. Bugárová, B.M. Todorović Marković, Antibacterial composite hydrogels of graphene quantum dots and bacterial cellulose accelerate wound healing, J Biomed Mater Res B Appl Biomater 110 (2022) 1796–1805, https://doi.org/10.1002/JBM.B.35037.

[14] Y. Liang, H. Xu, Z. Li, A. Zhangji, B. Guo, Bioinspired injectable self-healing hydrogel sealant with fault-tolerant and repeated thermo-responsive adhesion for sutureless post-wound-closure and wound healing, Nano-Micro Lett. 14 (2022) 1–19, https://doi.org/10.1007/S40820-022-00928-Z/FIGURES/8.

[15] R. Yu, H. Zhang, B. Guo, Conductive biomaterials as bioactive wound dressing for wound healing and skin tissue engineering, Nano-Micro Lett. 1 (14) (2021) 1–46 https://doi.org/10.1007/S40820-021-00751-Y, 2021 14.

[16] J. He, Z. Zhang, Y. Yang, F. Ren, J. Li, S. Zhu, F. Ma, R. Wu, Y. Lv, G. He, B. Guo, D. Chu, Injectable self-healing adhesive pH-responsive hydrogels accelerate gastric hemostasis and wound healing, Nano-Micro Lett. 13 (2021) 1–17, https://doi.org/10.1007/S40820-020-00585-0/FIGURES/6.

[17] J. Liu, M. Qu, C. Wang, Y. Xue, H. Huang, Q. Chen, W. Sun, X. Zhou, G. Xu, X. Jiang, A dual-cross-linked hydrogel patch for promoting diabetic wound healing, Small 18 (2022) 2106172, https://doi.org/10.1002/smll.202106172.

[18] Z. Ming, L. Han, M. Bao, H. Zhu, S. Qiang, S. Xue, W. Liu, Z. Ming, L. Han, M. Bao, H. Zhu, S. Qiang, S. Xue, W. Liu, Living bacterial hydrogels for accelerated infected wound healing, Adv. Sci. 8 (2021) 2102545, https://doi.org/10.1002/ADVS.202102545.

[19] X. Peng, Y. Li, T. Li, Y. Li, Y. Deng, X. Xie, Y. Wang, G. Li, L. Bian, Coacervate-derived hydrogel with effective water repulsion and robust underwater bioadhesion promotes wound healing, Adv. Sci. 9 (2022) 2203890, https://doi.org/10.1002/ADVS.202203890.

[20] S. Young Wang, H. Kim, G. Kwak, H. Yeol Yoon, S. Duk Jo, J. Eun Lee, D. Cho, I. Chan Kwon, S. Hwa Kim, S.Y. Wang, H. Kim, G. Kwak, H.Y. Yoon, S.D. Jo, J.E. Lee, I.C. Kwon, S.H. Kim, D. Cho, Development of biocompatible HA hydrogels embedded with a new synthetic peptide promoting cellular migration for advanced wound care management, Adv. Sci. 5 (2018) 1800852, https://doi.org/10.1002/ADVS.201800852.

[21] Z. Yang, R. Huang, B. Zheng, W. Guo, C. Li, W. He, Y. Wei, Y. Du, H. Wang, D. Wu, H. Wang, Z. Yang, R. Huang, W. Guo, C. Li, Y. Wei, Y. Du, H. Wang, B. Zheng, W. He, D. Wu, Highly stretchable, adhesive, biocompatible, and antibacterial hydrogel dressings for wound healing, Adv. Sci. 8 (2021) 2003627, https://doi.org/10.1002/ADVS.202003627.

[22] S. Faraji, N. Nowroozi, A. Nouralishahi, J. Shabani Shayeh, Electrospun polycaprolactone/graphene oxide/quercetin nanofibrous scaffold for wound dressing: evaluation of biological and structural properties, Life Sci. 257 (2020) 118062, https://doi.org/10.1016/J.LFS.2020.118062.

[23] N. Nowroozi, S. Faraji, A. Nouralishahi, M. Shahrousvand, Biological and structural properties of graphene oxide/curcumin nanocomposite incorporated chitosan as a scaffold for wound healing application, Life Sci. 264 (2021) 118640, https://doi.org/10.1016/J.LFS.2020.118640.

[24] Z. Wan, J. He, Y. Yang, T. Chong, J. Wang, B. Guo, L. Xue, Injectable adhesive self-healing biocompatible hydrogel for haemostasis, wound healing, and postoperative tissue adhesion prevention in nephron-sparing surgery, Acta Biomater. 152 (2022) 157–170, https://doi.org/10.1016/J.ACTBIO.2022.09.006.

[25] J. Chen, J. He, Y. Yang, L. Qiao, J. Hu, J. Zhang, B. Guo, Antibacterial adhesive self-healing hydrogels to promote diabetic wound healing, Acta Biomater. 146 (2022) 119–130, https://doi.org/10.1016/J.ACTBIO.2022.04.041.

[26] X. Qi, X. Tong, S. You, R. Mao, E. Cai, W. Pan, C. Zhang, R. Hu, J. Shen, Mild hyperthermia-assisted ROS scavenging hydrogels achieve diabetic wound healing, ACS Macro Lett. 11 (2022) 861–867, https://doi.org/10.1021/acsmacrolett.2c00290.

[27] S. You, Y. Huang, R. Mao, Y. Xiang, E. Cai, Y. Chen, J. Shen, W. Dong, X. Qi, Together is better: poly(tannic acid) nanorods functionalized polysaccharide hydrogels for diabetic wound healing, Ind. Crop. Prod. 186 (2022), https://doi.org/10.1016/j.indcrop.2022.115273.

[28] S. Iravani, R.S. Varma, Plants and plant-based polymers as scaffolds for tissue engineering, Green Chem. 21 (2019) 4839–4867, https://doi.org/10.1039/C9GC02391G.

[29] M. Olvera-Sosa, S. Rosales-Mendoza, G.S. García-Briones, M.D.L. Betancourt-Mendiola, O. González-Ortega, G. Palestino, A novel acrylic acid-schizochytrium sp. Bio-based polymer: design, synthesis, and properties, Mater. Today Commun. 26 (2021) 102029, https://doi.org/10.1016/J.MTCOMM.2021.102029.

[30] Y. Zhong, H. Xiao, F. Seidi, Y. Jin, Natural polymer-based antimicrobial hydrogels without synthetic antibiotics as wound dressings, Biomacromolecules 21 (2020) 2983–3006, https://doi.org/10.1021/ACS.BIOMAC.0C00760.

[31] M.M. Pillai, H. Dandia, R. Checker, S. Rokade, D. Sharma, P. Tayalia, Novel combination of bioactive agents in bilayered dermal patches provides superior wound healing, Nanomedicine 40 (2022) 102495, https://doi.org/10.1016/J.NANO.2021.102495.

[32] X. Liu, T.C. Tang, E. Tham, H. Yuk, S. Lin, T.K. Lu, X. Zhao, Stretchable living materials and devices with hydrogel-elastomer hybrids hosting programmed cells, Proc. Natl. Acad. Sci. U. S. A. 114 (2017) 2200–2205, https://doi.org/10.1073/PNAS.1618307114.

[33] Y. Liang, Z. Li, Y. Huang, R. Yu, B. Guo, Dual-dynamic-bond cross-linked antibacterial adhesive hydrogel sealants with on-demand removability for post-wound-closure and infected wound healing, ACS Nano 15 (2021) 7078–7093, https://doi.org/10.1021/ACSNANO.1C00204.

[34] M. Nurunnabi, Z. Khatun, K.M. Huh, S.Y. Park, D.Y. Lee, K.J. Cho, Y.K. Lee, In vivo biodistribution and toxicology of carboxylated graphene quantum dots, ACS Nano 7 (2013) 6858–6867, https://doi.org/10.1021/NN402043C.

[35] A.X. Zheng, Z.X. Cong, J.R. Wang, J. Li, H.H. Yang, G.N. Chen, Highly-efficient peroxidase-like catalytic activity of graphene dots for biosensing, Biosens. Bioelectron. 49 (2013) 519–524, https://doi.org/10.1016/J.BIOS.2013.05.038.

[36] X. Wu, F. Tian, W. Wang, J. Chen, M. Wu, J.X. Zhao, Fabrication of highly fluorescent graphene quantum dots using L-glutamic acid for in vitro/in vivo imaging and sensing, J Mater Chem C Mater 1 (2013) 4676–4684, https://doi.org/10.1039/C3TC30820K.

[37] Y. Zhang, C. Wu, X. Zhou, X. Wu, Y. Yang, H. Wu, S. Guo, J. Zhang, Graphene quantum dots/gold electrode and its application in living cell H2O2 detection, Nanoscale 5 (2013) 1816–1819, https://doi.org/10.1039/C3NR33954H.

[38] H. Sun, L. Wu, W. Wei, X. Qu, Recent advances in graphene quantum dots for sensing, Mater. Today 16 (2013) 433–442, https://doi.org/10.1016/J.MATTOD.2013.10.020.

[39] H. Sun, N. Gao, K. Dong, J. Ren, X. Qu, Graphene quantum dots-band-aids used for wound disinfection, ACS Nano 8 (2014) 6202–6210, https://doi.org/10.1021/NN501640Q/SUPPL_FILE/NN501640Q_SI_001.PDF.

[40] N. Wang, H. Xu, S. Sun, P. Guo, Y. Wang, C. Qian, Y. Zhong, D. Yang, Wound therapy via a photo-responsively antibacterial nano-graphene quantum dots conjugate, J. Photochem. Photobiol. B 210 (2020) 111978, https://doi.org/10.1016/J.JPHOTOBIOL.2020.111978.

[41] A. Mandal, J.R. Clegg, A.C. Anselmo, S. Mitragotri, Hydrogels in the clinic, Bioeng. Transl. Med. 5 (2020) e10158, https://doi.org/10.1002/BTM2.10158.

[42] A. Das, S. Basu, A. Verma, K. Scott, Characterization of low cost ion conducting Poly(AAc-co-DMAPMA) membrane for fuel cell application, Mater. Sci. Appl. 6 (2015), https://doi.org/10.4236/msa.2015.63028.

[43] S.K. Swain, K. Prusty, Biomedical applications of acrylic-based nanohydrogels, J. Mater. Sci. 53 (2018) 2303–2325, https://doi.org/10.1007/S10853-017-1726-X.

[44] S. Kundu, R.M. Yadav, T.N. Narayanan, M.V. Shelke, R. Vajtai, P.M. Ajayan, V.K. Pillai, Synthesis of N, F and S co-doped graphene quantum dots, Nanoscale 7 (2015) 11515–11519, https://doi.org/10.1039/C5NR02427G.

[45] M. Torres-Lugo, N.A. Peppas, Molecular design and in vitro studies of novel pH-sensitive hydrogels for the Oral delivery of calcitonin, Macromolecules 32 (1999) 6646–6651, https://doi.org/10.1021/MA990541C.

[46] M. Calvaresi, M. Quintana, P. Rudolf, F. Zerbetto, M. Prato, Rolling up a

graphene sheet, ChemPhysChem 14 (2013) 3447–3453, https://doi.org/10.1002/CPHC.201300337.
[47] A. Singh, R. Bhattacharya, A. Shakeel, A.K. Sharma, S. Jeevanandham, A. Kumar, S. Chattopadhyay, H.B. Bohidar, S. Ghosh, S. Chakrabarti, S.K. Rajput, M. Mukherjee, Hydrogel nanotubes with ice helices as exotic nanostructures for diabetic wound healing, Mater. Horiz. 6 (2019) 274–284, https://doi.org/10.1039/C8MH01298A.
[48] H. Chen, Y. Cheng, J. Tian, P. Yang, X. Zhang, Y. Chen, Y. Hu, J. Wu, Dissolved oxygen from microalgae-gel patch promotes chronic wound healing in diabetes, Sci. Adv. 6 (2020), https://doi.org/10.1126/SCIADV.ABA4311.
[49] Y. Guan, H. Niu, Z. Liu, Y. Dang, J. Shen, M. Zayed, L. Ma, J. Guan, Sustained oxygenation accelerates diabetic wound healing by promoting epithelialization and angiogenesis and decreasing inflammation, Sci. Adv. 7 (2021), https://doi.org/10.1126/SCIADV.ABJ0153.
[50] M.L. Obaíd, J.P. Camacho, M. Brenet, R. Corrales-Orovio, F. Carvajal, X. Martorell, C. Werner, V. Simón, J. Varas, W. Calderón, C.D. Guzmán, M.R. Bono, S. San Martín, A. Eblen-Zajjur, J.T. Egaña, A first in human trial implanting microalgae shows safety of photosynthetic therapy for the effective treatment of full thickness skin wounds, Front. Med. 8 (2021), https://doi.org/10.3389/FMED.2021.772324.
[51] S. You, Y. Xiang, X. Qi, R. Mao, E. Cai, Y. Lan, H. Lu, J. Shen, H. Deng, Harnessing a biopolymer hydrogel reinforced by copper/tannic acid nanosheets for treating bacteria-infected diabetic wounds, Mater. Today Adv. 15 (2022) 100271, https://doi.org/10.1016/J.MTADV.2022.100271.
[52] Z.P. Li, S. You, R. Mao, Y. Xiang, E. Cai, H. Deng, J. Shen, X. Qi, Architecting polyelectrolyte hydrogels with cu-assisted polydopamine nanoparticles for photothermal antibacterial therapy, Mater. Today Bio. 15 (2022) 100264, https://doi.org/10.1016/J.MTBIO.2022.100264.
[53] X. Qi, Y. Xiang, E. Cai, S. You, T. Gao, Y. Lan, H. Deng, Z.P. Li, R. Hu, J. Shen, All-in-one: harnessing multifunctional injectable natural hydrogels for ordered therapy of bacteria-infected diabetic wounds, Chem. Eng. J. 439 (2022) 135691, https://doi.org/10.1016/J.CEJ.2022.135691.
[54] B. Stubbe, A. Mignon, H. Declercq, S. Van Vlierberghe, P. Dubruel, Development of gelatin-alginate hydrogels for burn wound treatment, Macromol. Biosci. 19 (2019), https://doi.org/10.1002/MABI.201900123.
[55] K. Kalantari, E. Mostafavi, B. Saleh, P. Soltantabar, T.J. Webster, Chitosan/PVA hydrogels incorporated with green synthesized cerium oxide nanoparticles for wound healing applications, Eur. Polym. J. 134 (2020) 109853, https://doi.org/10.1016/J.EURPOLYMJ.2020.109853.
[56] A. Rafieerad, W. Yan, G.L. Sequiera, N. Sareen, E. Abu-El-Rub, M. Moudgil, S. Dhingra, Application of Ti3C2 MXene quantum dots for immunomodulation and regenerative medicine, Adv. Healthc. Mater. 8 (2019) 1900569, https://doi.org/10.1002/ADHM.201900569.
[57] H. Sun, N. Gao, K. Dong, J. Ren, X. Qu, Graphene quantum dots-band-aids used for wound disinfection, ACS Nano 8 (2014) 6202–6210, https://doi.org/10.1021/NN501640Q.
[58] X. Zhong, C. Tong, T. Liu, L. Li, X. Liu, Y. Yang, R. Liu, B. Liu, Silver nanoparticles coated by green graphene quantum dots for accelerating the healing of MRSA-infected wounds, Biomater. Sci. 8 (2020) 6670–6682, https://doi.org/10.1039/D0BM01398F.
[59] A.A. Romoser, P.L. Chen, J.M. Berg, C. Seabury, I. Ivanov, F.M.F. Criscitiello Michael, C.M. Sayes, Quantum dots trigger immunomodulation of the NFκB pathway in human skin cells, Mol. Immunol. 48 (2011) 1349–1359, https://doi.org/10.1016/J.MOLIMM.2011.02.009.
[60] C. Wang, M. Wang, T. Xu, X. Zhang, C. Lin, W. Gao, H. Xu, B. Lei, C. Mao, Engineering bioactive self-healing antibacterial exosomes hydrogel for promoting chronic diabetic wound healing and complete skin regeneration, Theranostics 9 (2019) 65, https://doi.org/10.7150/THNO.29766.